Effect of Anti-C5a Therapy in a Murine Model of Early/Intermediate Dry Age-Related Macular Degeneration

Christopher B. Toomey,[1–3] Michael Landowski,[1] Mikael Klingeborn,[1] Una Kelly,[1] John Deans,[1] Holly Dong,[4] Ons Harrabi,[4] Thomas Van Blarcom,[4] Yik Andy Yeung,[4] Ruslan Grishanin,[4] John C. Lin,[4] Daniel R. Saban,[1,5] and Catherine Bowes Rickman[1,2]

[1]Department of Ophthalmology, Duke University Medical Center, Durham, North Carolina, United States
[2]Department of Cell Biology, Duke University Medical Center, Durham, North Carolina, United States
[3]Shiley Eye Institute, Department of Ophthalmology, University of California-San Diego, San Diego, California, United States
[4]Rinat, Pfizer Inc, South San Francisco, California, United States
[5]Department of Immunology, Duke University Medical Center, Durham, North Carolina, United States

Correspondence: Catherine Bowes Rickman, Duke University Medical Center, Box 3802, AERI Rm 5010, Durham, NC 27710, USA; bowes007@duke.edu.

CBT and ML contributed equally to the work presented here and should therefore be regarded as equivalent authors.

Submitted: October 11, 2017
Accepted: December 25, 2017

Citation: Toomey CB, Landowski M, Klingeborn M, et al. Effect of anti-C5a therapy in a murine model of early/intermediate dry age-related macular degeneration. *Invest Ophthalmol Vis Sci*. 2018;59:662–673. https://doi.org/10.1167/iovs.17-23134

Purpose. A large body of evidence supports a central role for complement activation in the pathobiology of age-related macular degeneration (AMD), including plasma complement component 5a (C5a). Interestingly, C5a is a chemotactic agent for monocytes, a cell type also shown to contribute to AMD. However, the role monocytes play in the pathogenesis of "dry" AMD and the pharmacologic potential of targeting C5a to regulate these cells are unclear. We addressed these questions via C5a blockade in a unique model of early/intermediate dry AMD and large panel flow cytometry to immunophenotype monocytic involvement.

Methods. Heterozygous complement factor H ($Cfh^{+/-}$) mice aged to 90 weeks were fed a high-fat, cholesterol-enriched diet ($Cfh^{+/-}$~HFC) for 8 weeks and were given weekly intraperitoneal injections of 30 mg/kg anti-C5a (4C9, Pfizer). Flow cytometry, retinal pigmented epithelium (RPE) flat mounts, and electroretinograms were used to characterize anti-C5a treatment.

Results. Aged $Cfh^{+/-}$ mice developed RPE damage, sub-RPE basal laminar deposits, and attenuation of visual function and immune cell recruitment to the choroid that was accompanied by expression of inflammatory and extracellular matrix remodeling genes following 8 weeks of HFC diet. Concomitant systemic administration of an anti-C5a antibody successfully inhibited local recruitment of mononuclear phagocytes to the choroid–RPE interface but did not ameliorate these AMD-like pathologies in this mouse model.

Conclusions. These results show that immunotherapy targeting C5a is not sufficient to block the development of the AMD-like pathologies observed in $Cfh^{+/-}$~HFC mice and suggest that other complement components or molecules/mechanisms may be driving "early" and "intermediate" AMD pathologies.

Keywords: complement, age related macular degeneration, immunotherapy, monocytosis

Age-related macular degeneration (AMD) is a leading cause of legal blindness in elderly persons in developed countries and has limited therapeutic options.[1–4] Multiple studies have linked activation of the complement cascade, in particular the alternative complement pathway (alternative pathway), with AMD development and progression.[5] Many components of the alternative pathway are found in the protein- and lipid-rich deposits occurring between the retinal pigmented epithelium (RPE) and Bruch's membrane (BrM), which are known as drusen and define AMD pathohistology.[6–9] In addition, polymorphisms in complement factor H (*CFH*), a key negative regulator of the alternative pathway, are responsible for a significant portion of the genetic attributable risk of AMD.[10] These lines of evidence support the hypothesis that overactivation of the alternative pathway predisposes the posterior eye to AMD development and progression. In fact, intravitreal injections of lampalizumab, an inhibitor for the positive regulator of the alternative pathway, Factor D, showed promise as a therapy for late "dry" AMD or geographic atrophy but failed to meet the primary endpoint during its first of two phase III clinical trials.[11] However, it is unknown whether there are still residual activated complement components either from incomplete blockade of the alternative pathway or from activation of the classical pathway that may explain the recent failure of lampalizumab as an AMD therapy.

Early/intermediate dry AMD is characterized by impaired dark adaptation reflecting rod photoreceptor dysfunction, RPE pigmentary changes, and the presence of intermediate-sized (63–124 μm) drusen.[12] We have recently developed a novel murine model of early/intermediate dry AMD based on multiple risk factors associated with AMD: advanced age, alternative pathway dysregulation, and environmental stress.[13] Male heterozygous complement factor H knockout ($Cfh^{+/-}$) mice aged to 90 weeks and fed an 8-week high-fat, cholesterol-enriched (HFC) diet develop attenuated rod-mediated visual function, increased RPE damage, and increased sub-RPE basal laminar deposits, while age-matched homozygous *Cfh* knockout ($Cfh^{-/-}$) mice fed a HFC diet develop only increased sub-

RPE basal laminar deposits.[13] Since aged *Cfh*$^{-/-}$ mice lack an intact complement system we hypothesize that the decreased visual function and increased RPE damage observed in the *Cfh*$^{+/-}$ mice are due to HFC-induced complement activation.[13,14] Supporting this hypothesis, we observed an increase in plasma complement component 5a (C5a) in aged *Cfh*$^{+/-}$ mice on a HFC diet (*Cfh*$^{+/-}$∼HFC) compared to aged *Cfh*$^{-/-}$ mice on a HFC diet (*Cfh*$^{-/-}$∼HFC).[13]

C5a is a critical chemoattractant protein responsible for the recruitment, activation, and maintenance of immune cells.[15] Consequently, we observed an increase in extravascular recruitment of mononuclear phagocytes (MNPs) to the RPE/choroid in aged *Cfh*$^{+/-}$∼HFC compared to *Cfh*$^{-/-}$∼HFC mice, suggesting a potential role of C5a in the development of AMD-like pathologies seen in this dry AMD model.[13] C5a is increased in the plasma of AMD patients[16–18] and is a constituent of drusen.[8] C5a was shown to increase the expression of proteins in tissues implicated in AMD such as intercellular adhesion molecule-1 (ICAM1),[19] interleukin-17 (IL-17),[20] interleukin-18 (IL-18),[21] interleukin-22 (IL-22),[20] and vascular endothelial growth factor a (VEGF-A).[22] Intraocular injections of antibodies or receptor trap targeting VEGF-A such as bevacizumab, aflibercept, and ranibizumab are current standard treatments for patients with "wet" AMD, a late manifestation of AMD characterized by choroidal neovascularization (CNV). Similarly, antibodies and an aptamer targeting C5a have decreased the lesion size in the acute laser-induced CNV mouse model of wet AMD and show promise as a potential therapy for wet AMD.[8,23,24]

In this study, we tested the role of C5a in the development of early/intermediate AMD-like pathology because therapies targeting C5a have been used successfully to reduce damage in a wet AMD mouse model.[8,23,24] Aged *Cfh*$^{+/-}$ mice fed a HFC diet were treated with weekly systemic injections of an anti-C5a antibody (4C9; Pfizer, San Francisco, CA, USA). Although anti-C5a therapy has a significant effect in an acute model of retinal degeneration and neovascularization, it did not appear to protect *Cfh*$^{+/-}$∼HFC mice from the development of early/intermediate dry AMD-like features, including reduced electroretinogram (ERG) responses, increased RPE damage, increased sub-RPE basal laminar deposits, and increased inflammatory and extracellular matrix (ECM) gene expression. Since C5a acts as a chemoattractant and C5a receptor 1 (*C5aR1*) expression is confined to the choroid in the eye, we quantified immune cell populations in the RPE/choroid after anti-C5a therapy and found reduced MNP recruitment in treated aged *Cfh*$^{+/-}$∼HFC mice. These results establish that the blockade of C5a is not sufficient to protect mice from the development of early/intermediate dry AMD-like pathologies in aged *Cfh*$^{+/-}$∼HFC despite blocking the recruitment of MNPs to the RPE/choroid. This observation is in contrast to previous studies as well as our findings that C5a blockade appears to be an efficacious mono- or combinatorial therapy with anti-VEGF for models of wet AMD.

Materials and Methods

Mice

Mice were housed and maintained in accordance with the Institutional Animal Care and Use Committee at Duke University in adherence with the ARVO Statement for the Use of Animals in Ophthalmic and Vision Research. *Cfh*$^{+/-}$ mice were generated as previously described.[14] We confirmed that none of the mice carried the rd8 mutation.[25] Aged male *Cfh*$^{+/-}$ mice (n = 67; 91–110 weeks) were maintained on a normal rodent chow diet (normal diet [ND], Isopurina 5001; Prolab, Dewitt, NY, USA), and a subset of cage- and littermate mice were switched to a HFC diet (n = 38; TD 88051; Envigo, Madison, WI, USA) for 8 weeks. Mice were randomly assigned to treatment groups with an even distribution by age.

For studies using the laser-induced CNV or the sodium iodate ($NaIO_3$) models, male C57BL/6J aged 8 to 10 weeks were obtained from The Jackson Laboratory (Sacramento, CA, USA). A total of 6 to 12 mice were used per dosing group (n = 78 total/model). The care and use of mice for both of these studies adhered to Pfizer's Institutional Animal Care and Use Committee guidelines.

C5a and VEGF Antibodies

The anti-C5a antibody, 4C9, was isolated from a phage displayed single chain antibody variable fragment (scFv) library derived from human donors and was provided as a gift from Laird Bloom of Pfizer, Inc. It binds to human and mouse C5a with low nanomolar affinity and blocks binding of C5a to the C5a receptor (C5aR). The affinity of this antibody toward C5a was increased using a yeast surface display system; the resulting higher-affinity clone was subsequently used in the study described here. In brief, the antibody was cloned as a scFv into a yeast display vector[26] and then CDRH2, CDRH3, CDRL1, and CDRL3 of the antibody were individually mutated using look-through mutagenesis.[27] *S. cerevisiae* BJ5465 harboring the library was subjected to three rounds of fluorescence-activated cell sorting (FACS) with gating strategies designed to isolate higher-affinity clones.[28] DNA encoding the enriched clones was randomly combined and subjected to three additional rounds of FACS followed by individual screening. A higher-affinity clone was identified, expressed as a chimeric monoclonal antibody (human VH and VL domains fused to mouse IgG1 heavy chain and kappa light chain constant regions) in HEK293F cells, purified using standard techniques, binding with human and mouse C5a determined by surface plasmon resonance (SPR) (Biacore, GE Healthcare, Piscataway, NJ, USA), and then used in this study.

Mouse anti-VEGF-A antibody was constructed as murine IgG1 based on the published sequences of the G6-31 antibody (patent CA2533297A1[29]) that was previously shown to bind both mouse and human VEGF with high affinity.[29] In brief, the sequences of variable regions of G6-31 were synthesized, cloned into the mouse IgG1 heavy chain and kappa light chain, expressed in the HEK293F cells, and purified using standard techniques, and its interaction with mouse VEGF-A was confirmed by SPR (Biacore, GE Healthcare).

$NaIO_3$ Treatment and Anti-C5a Dose Response (4C9)

$NaIO_3$ treatment was performed as previously described in order to determine the appropriate dose of anti-C5a therapy needed to observe a therapeutic effect in the posterior eye.[30] Briefly, 8- to 10-week-old C57BL/6J mice were injected into the intraperitoneal (IP) space with 3, 10, 20, 30, or 60 mg/kg anti-C5a or 60 mg/kg isotype control (day −1). The next day, mice were intravenously injected with 25 mg/kg $NaIO_3$ or PBS control (day 0). On day 2, mice were dark adapted for 24 hours, and on day 3, ERGs were performed as described below at flash intensities of 1E-4, 1E-3, 1E-1, and 2.5 (cd*s/m^2).

Antibody C5a Treatment of *Cfh* Mice and Laser CNV Model

Cfh$^{+/-}$ mice were treated with 30 mg/kg anti-C5a via a weekly IP injection. Injections began at the onset of HFC diet and were continued during the 8 weeks of diet.

For the laser CNV model, 30 mg/kg anti-C5a was administered with or without anti-VEGF at 3, 5, or 10 mg/kg 1 day prior to CNV induction and at days 5 and 11 post laser CNV.

Laser-Induced CNV Model

Experimental CNV was induced bilaterally in C57BL/6J mice at 8 to 10 weeks of age. Animals were anesthetized with IP injection of ketamine (60 mg/kg) and xylazine (9 mg/kg). Animals were pretreated with 1% atropine (atropine sulfate, 1 drop) and tropicamide (1%, 1 drop) eye drops. A coverslip was placed over the cornea with a large drop of Goniosol. Three 532-nm diode laser pulses with a spot size of 50 μm, duration of 0.1 second, and power of 110 mW (OcuLight TX; IRIDEX, Mountain View, CA, USA) were applied between retinal vessels at 12, 4, and 8 o'clock, two disc diameters from the optic nerve, with the use of a slit-lamp and ophthalmologic microscope (SL980/5X; IRIDEX). Formation of a bubble at the time of laser application, which indicates rupture of BrM, was an important factor in obtaining laser-induced CNV.[31] Only laser burns in which a bubble was produced were included in the study. Any lesions that did not yield the characteristic white "bubble" formation or any hemorrhaging lesions automatically resulted in removal of the animal from the study. A total of 6 to 12 mice were used per dosing group.

Analysis of CNV by Scanning Laser Angiography

Angiography was performed at day 12 post laser treatment with a scanning laser ophthalmoscope (SLO) using the Spectralis Heidelberg Retina Tomograph (HRT)/SLO (Heidelberg Engineering, Dossenheim, Germany), which was used as a digital confocal SLO (cSLO) since it is equipped with four laser wavelengths (488, 514, 788, and 820 nm) and filters for fluorescein and indocyanine green (ICG) fluorescence. To adapt the commercial system to the optics of the mouse eye, we used a 55-diopter lens as a front objective (Linos Optics, Milford, MA, USA) instead of the 40-mm focal lens used for a human eye. Pupils were dilated with topical 1% atropine. Mice were anesthetized by IP injection of ketamine (60 mg/kg) and xylazine (9 mg/kg) and kept on a heated pad during the procedure. Plasma labeling by sodium fluorescein (Akorn, Inc., Lake Forest, IL, USA) was used for choroidal vessel imaging. Five hundred microliters of 2 mg/mL sterile sodium fluorescein solution was injected IP 8 minutes prior to cSLO imaging. Following the recordings, mice were kept in the cage placed on a warming pad until they recovered from anesthesia.

Quantitative CNV Lesion Analysis

In order to analyze the fluorescein fundus angiography, image analysis was performed with open-source software, ImageJ (National Institutes of Health, Bethesda, MD, USA). A masked grader performed quantification of the CNV lesion size. In brief, for the quantification, raw images of angiography were imported into ImageJ and the CNV lesion was demarcated using the freehand selection tool, avoiding large vessels. The volume and brightness of the lesions were quantitated with background optical density from the neighboring to CNV region subtracted as arbitrary units. Analysis of variance and post hoc *t*-test were used to assess the statistical significance between the treatment groups.

Anti-C5a ELISA

Anti-C5a (4C9) levels were determined by ELISA. Briefly, mC5a (no. 2150-c5; R&D Systems, Minneapolis, MN, USA) was incubated at 4°C overnight in 96-well plates. After washing unbound protein and blocking with 2% BSA, a 1:1000 dilution of plasma was incubated overnight at 4°C. Following wash steps, the plate was sequentially incubated with biotinylated anti-mouse IgG (H and L) HRP (1:3000; BD Biosciences, San Jose, CA, USA), TMB substrate reagent (BD Biosciences) and the OD 450 nm read; 0.31 to 200 ng/mL anti-C5a (4C9) was used as a standard curve.

Analysis of Sub-RPE Basal Laminar Deposits by Transmission Electron Microscopy

Quantification of sub-RPE basal laminar deposits was performed as previously described.[32] Briefly, thin sections of 60 to 80 nm were cut from sections obtained from the center of the posterior eyecup and stained with uranyl acetate and Sato's lead. Images containing the basal RPE and BrM were taken on the parts of the section adjacent to the grid's bar throughout the length of the retina. For each image, the thickness of the deposits was measured from the central elastin layer of BrM to the top of the deposit using ImageJ software.

Analysis of RPE Damage Based on Flat Mount Quantification of Multinucleated Cells

RPE flat mount preparation was performed as previously described.[13] Briefly, RPE flat mounts were stained with a rabbit antibody against zona occludens-1 (ZO-1) (40–2200, 1:100; Invitrogen, Carlsbad, CA, USA) and Hoechst 33342, and confocal images were captured on a Nikon Eclipse C1 microscope (New York, NY, USA). Morphometric analysis was performed by a masked grader from each central quadrant. The number of enlarged, multinucleated (nuclei ≥ 3) cells per central field view was counted.

In Vivo Visual Function Analysis by Electroretinography

Electroretinography was performed as previously described.[13] Briefly, mice were dark adapted overnight; pupils were dilated with 0.5% tropicamide and 1.25% phenylephrine, and mice were anesthetized with a mixture of ketamine (100 mg/kg) and xylazine (10 mg/kg). Scotopic ERGs were recorded using an Espion E2 system (Diagnosys LLC, Lowell, MA, USA) at increasing flash intensities. The data points from the b-wave stimulus-response curves were fitted using the least-square fitting procedure (OriginPro 9.0; OriginLab, Northampton, MA, USA).

Inflammation and Extracellular Matrix Pathway-Focused RNA Arrays

Total RNA from four eyecups (RPE/choroid/sclera) from each $Cfb^{+/-}$ group was extracted using an RNeasy lipid tissue mini kit (Qiagen, Inc., Valencia, CA, USA) according to the manufacturer's instructions. RNA concentrations were determined using the Nanodrop 2000 UV-Vis Spectrophotometer (Thermo Scientific, Waltham, MA, USA). Eyecup RNA (600 ng) was used to synthesize cDNA using the RT^2 First Strand cDNA kit (Qiagen, Inc.). cDNA was combined with RT^2 SYBR Green qPCR Mastermix (Qiagen, Inc.) and Ultrapure RNAse/DNAse-free water (Invitrogen). Real-time PCR data analysis of the cDNA was performed on two mouse RT^2 PCR pathway-focused arrays from Qiagen, Inc. (RT^2 Profiler: Inflammatory Response and Autoimmunity [cat. no. PAMM-077ZD] and Extracellular Matrix and Adhesion Molecule [cat. no. PAMM-013ZD]) following the manufacturer's protocol. Prior to RNA expres-

sion analysis, quality controls for genomic contamination, reverse transcription, and positive PCR were checked for each plate to confirm that each plate met quality controls. Relative mRNA expression was normalized to five endogenous reference genes, *Actb*, *B2m*, *Gapdh*, *GusB*, and *Hsp90ab1*, for each group using the quantitative $2^{-\Delta\Delta C}{}_T$ method.[33] All the expression data for the Inflammatory Response and Autoimmunity and the Extracellular Matrix and Adhesion Molecule arrays are presented in Supplementary Tables S1 and S2, respectively. For these analyses, a gene was considered to be upregulated or downregulated if the fold change was greater than 1.25 as previously described[34] and shown in Supplementary Figure S2.

Expression of individual genes was examined in triplicate reactions using 25 ng cDNA from a pooled RNA sample consisting of four eyecups from each group ($Cfh^{+/-}$~ND, $Cfh^{+/-}$~HFC, and $Cfh^{+/-}$~HFC + antiC5a), 200 nmol/L each primer, and 12.5 µL iQTM SYBR green supermix (Bio-Rad, Hercules, CA, USA) in 25 µL total volume. Primer sequences used in this study are shown in Supplementary Table S3. RT-PCR reactions were run in the CFX96 system (Bio-Rad) at 95°C for 3 minutes, followed by 40 cycles at 95°C for 10 seconds and 60°C for 20 seconds, then 72°C for 15 seconds. Relative mRNA expression was normalized to the endogenous reference murine gene ribosomal protein lateral stalk subunit P0 (*Rlpl0*) using the quantitative $2^{-\Delta\Delta C}{}_T$ method.[33]

Tissue and RNA Isolation, and RT-PCR

Three C57BL/6J mice were euthanized with CO_2 and perfused with 15 mL PBS. After perfusion, eyes were enucleated for dissection where fat, muscle, and anterior segment were removed. Neural retina was carefully separated from the posterior eyecup, placed into a separate Eppendorf tube, and flash frozen. RPE cells were isolated using a modified protocol described previously.[35] Briefly, RPE/choroid/sclera was placed into an Eppendorf tube with 1 mL RNAprotect Cell Reagent (Qiagen, Inc.) and left overnight at 4°C. The next day, choroid/sclera was removed, rinsed with PBS, and placed in a separate Eppendorf tube for RNA isolation. RPE cells were spun and RNAprotect was removed from tube. Both choroid/sclera and RPE tissues were flash frozen. Human RPE cells from a 71-year-old male human donor eye with a 3.5-hour procurement time were isolated by cutting the eye around the ora serrata, removing the vitreous and retina, then adding 500 µL cold PBS to the eyecup and gently rubbing with a rounded glass rod; this step was repeated. The cells were centrifuged at 4° for 10 minutes at 600*g*; the intact RPE cell pellet was washed one time with cold PBS and spun, the supernatant was removed, and cells were frozen at −80°. More rigorous washing and mechanical scraping of the eyecup removed any remaining RPE in the eyecup; then a portion, free of RPE cells, was cut out and the BrM and choroid were peeled from the sclera. This "choroid" sample was immediately frozen. Total RNA from each of these tissues, isolated from murine retina, RPE, and choroid/sclera as well as human RPE and choroid, was extracted using an RNeasy lipid tissue mini kit (Qiagen, Inc.) according to the manufacturer's instructions. RNA concentrations were determined using the Nanodrop 2000 UV-Vis Spectrophotometer (Thermo Scientific). RNA from ARPE-19 cells was generously provided by Goldis Malek (Duke University) and was isolated as previously described.[36] RNA (150 ng) from each sample was used to synthesize cDNA using ProtoScript II Reverse Transcriptase (NEB, Ipswich, MA, USA). Each RT-PCR reaction contained 7.5 ng cDNA, 200 nmol/L each primer, and 12.5 µL iQ SYBR green supermix (Bio-Rad) in 25 µL total volume. All primers used in this study span an exon–exon splice junction and are described in Supplementary Table S3. RT-PCR reactions were run in triplicate in the CFX96 system at 95°C for 3 minutes, followed by 40 cycles at 95°C for 10 seconds and 60°C for 20 seconds, then 72°C for 15 seconds. Relative mRNA expression was normalized to the endogenous reference gene beta-actin using the quantitative $2^{-\Delta\Delta C}{}_T$ method.[33]

Peripheral Blood and Extravascular RPE/Choroid MNP Analysis by Flow Cytometry

Intravascular staining of circulating immune cells was performed to differentiate circulating immune cells within the blood vessel from the extravascular immune cells that had migrated into the tissue of the posterior eye as previously described.[13,37] Briefly, 5 minutes prior to euthanasia, mice were injected retro-orbitally with 3 µg/50 µL APC/Cy7 anti-mouse CD45 (BioLegend, San Diego, CA, USA) (CD45-IV) to label the intravascular immune cells. Peripheral blood samples were subjected to red blood cell lysis and staining for cell viability (no. 65-0863; eBiosciences, San Diego, CA, USA) and labeled with antibodies against CD45 (no. 110735, BioLegend), CD11b (no. 562950, BD Biosciences), CD115 (no. 61-1152, eBiosciences), CD43 (no. 562866; BD Pharmingen, San Jose, CA, USA), Ly6C (no. 128022, BioLegend), and Ly6G (no. 127621, BioLegend) to determine the percent of classical and nonclassical monocytes per CD45+ cells based on established methods.[13,38] Both eyes were enucleated, retina was removed, and the RPE/choroid/sclera from each eye was isolated by microdissection. The RPE/choroid was mechanically removed from the subadjacent sclera. Six eyes were pooled to obtain cell numbers sufficient for analysis. RPE/choroid samples then underwent DNase I and collagenase treatment with mechanical stimulation to free immune cells. Subsequently samples were filtered and stained for cell viability, and labeled with antibodies against CD11b, CD45, Ly6C, Ly6G, CCR2 (R&D Systems, no. FAB5538A), CD11c (BD Biosciences, no. 563048), CD64 (BioLegend, no. 139308), F4/80 (BioLegend, no. 123109), and I-A/E (BioLegend, no. 107629). All samples were run on a BD Biosciences Fortessa flow cytometer using BD FACSDiva software (BD Biosciences). Gating is shown in figures and was performed as previously described in RPE/choroid.[13] With $N = 6$ eyes per group, two independent experiments were performed to confirm the data trend; the average of the peripheral blood analysis experiments is presented, and a representative experiment of the RPE/choroid data is presented. χ^2 statistical test for $P < 0.05$ was used to determine the statistical significance of the cell population frequencies normalized to total in the intra- or extravascular space CD45+ cells for a pooled sample.

Results

Anti-C5a Dosage and Efficacy in an Acute Model of Retinal Degeneration and of Neovascularization

The dose response of our novel mouse monoclonal anti-C5a antibody, 4C9, was determined in the $NaIO_3$ model of retinal degeneration.[30,39] Administration of $NaIO_3$ results in the ablation of scotopic b-wave in C57BL/6J mice.[40] ERGs were performed 3 days after mice were treated with either an intravenous injection of 3, 10, 20, 30, or 60 mg/kg anti-C5a or 60 mg/kg isotype control and were then subjected to an intravenous injection of $NaIO_3$. We observed a statistically significant rescue in ERG responses in mice receiving the 20, 30, and 60 mg/kg doses of anti-C5a at the 0.1 ($P < 0.05$) and 2.5 ($P < 0.001$) cd*s/m^2 flash intensity (Fig. 1A).

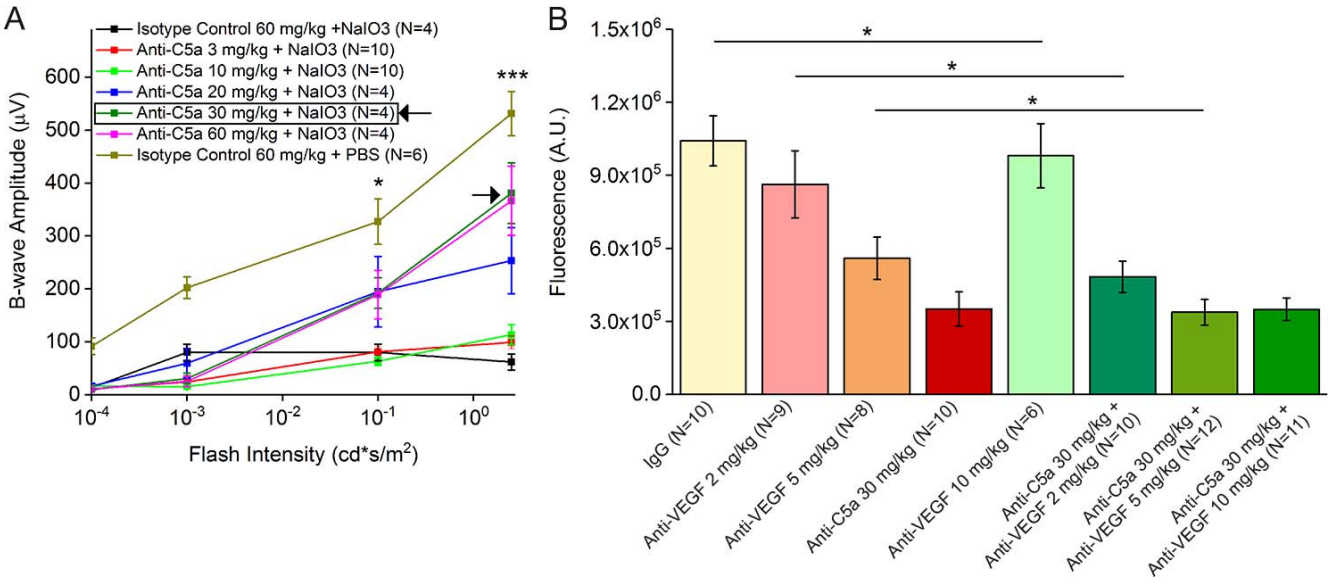

Figure 1. C5a dosage and efficacy studies using the sodium iodate ($NaIO_3$) model of retinal degeneration and laser-induced CNV model of wet AMD. (**A**) C5a dose–response therapy following $NaIO_3$. To determine the in vivo dose response of anti-C5a (4C9) in the context of posterior eye inflammation, mice were treated with increasing concentrations of anti-C5a (3, 10, 20, 30, and 60 mg/kg) or 60 mg/kg isotype control (Iso 60 mg/kg), delivered by a single injection IP, followed by the intravenous injection of $NaIO_3$ at 25 mg/kg. Scotopic electroretinogram (ERG) B-wave amplitudes are presented at increasing flash intensities of light. Mice receiving 20, 30, and 60 mg/kg doses of anti-C5a therapy had significantly higher ERG amplitudes than those receiving a PBS injection following $NaIO_3$ treatment. The *asterisks* (* and ***) represent statistical significance by ANOVA comparing treatments with post hoc Tukey test comparing 20, 30, or 60 mg/kg anti-C5a–treated mice to PBS-treated mice after $NaIO_3$ at $P < 0.05$ and $P < 0.001$, respectively. We chose the intermediate therapeutic dose of 30 mg/kg for our studies (*arrow*). *N* , number of mice. (**B**) The efficacy of the 30 mg/kg dosage of anti-C5a therapy was confirmed using the laser-induced choroidal neovascularization (CNV) mouse model. CNV lesion size was assessed following administration of either IgG isotype control or anti-C5a alone or in combination with anti-VEGF. Individual lesions were quantitated via ImageJ and arbitrary units per lesion were plotted. *Asterisk* (*) indicates statistical significance using the Student's *t*-test for $P < 0.05$ comparing IgG control or anti-VEGF at various doses in combination with 30 mg/kg anti-C5a therapy.

We validated the intermediate anti-C5a dosage (30 mg/kg) in the laser-induced CNV model for wet AMD.[41,42] The antiangiogenic effects of anti-C5a therapy were measured by fluorescein angiography in the rodent CNV model by scanning laser ophthalmoscopy. Neovascular lesion size was measured following administration of either anti-C5a and/or the standard of care, anti-VEGF, in a dose–response manner. Lesion size was used to determine whether (1) the anti-C5a antibody alone reduces CNV lesion size and (2) combination therapy with anti-VEGF synergizes with complement blockade to further enhance the therapeutic effect of VEGF inhibition (Supplementary Fig. S1). Anti-C5a therapy significantly reduced CNV lesion size in mice compared to IgG control at 30 mg/kg ($P < 0.05$) (Fig. 1B). In addition, administration of 30 mg/kg anti-C5a, as a combinatorial therapy, significantly enhanced the efficacy of subtherapeutic doses of anti-VEGF at 2 and 5 mg/kg ($P < 0.05$) (Fig. 1B). Thus, the anti-C5a antibody is able to reduce CNV lesion size as a monotherapy and as a combination therapy with anti-VEGF as supported by others.[8,23,24]

Anti-C5a Treatment in Aged *Cfh*$^{+/-}$∼HFC Mice

In our previous study of aged *Cfh*$^{+/-}$ and *Cfh*$^{-/-}$ mice fed a HFC diet we observed a striking correlation between complement dysregulation and RPE damage and visual function impairment.[13] These findings make the *Cfh*$^{+/-}$∼HFC a suitable model to test the effects of C5a with an anti-C5a therapy on early/intermediate dry AMD-like features. *Cfh*$^{+/-}$ mice aged at least 90 weeks were switched to a HFC diet and administered weekly IP injections of 30 mg/kg anti-C5a for 8 weeks. Plasma anti-C5a antibody levels ranged from 119 to 179 μg/mL 24 hours post injection, and after 7 days, antibody levels ranged from 58 to 99 μg/mL (Fig. 2A). Following 8 weeks of weekly IP injections, anti-C5a levels ranged from 153 to 80 μg/mL (mean of 99.4 μg/mL ± 26.8) 24 hours post final injection (Fig. 2B). Thus, sufficiently high plasma levels were maintained throughout the 8 weeks of HFC diet treatment in *Cfh*$^{+/-}$∼HFC mice.

Anti-C5a Therapy Does Not Reduce Early/Intermediate Dry AMD-Like Features in *Cfh*$^{+/-}$∼HFC Model

Extracellular lesions that form between the RPE and BrM characterize early AMD.[43] The effect of anti-C5a therapy on the thickness of sub-RPE basal laminar deposits that accumulate in *Cfh*$^{+/-}$∼HFC mice was analyzed by quantitative electron microscopy of RPE/BrM as previously described.[32] As we have previously shown, the majority of the sub-RPE deposits seen in the *Cfh*$^{+/-}$∼HFC model were 2- to 3-μm basal laminar deposits, and this did not change following anti-C5a therapy (Fig. 3A).[13] Quantitative analysis of sub-RPE basal laminar deposit thickness confirmed that anti-C5a therapy did not affect the amount of sub-RPE basal laminar deposits that accumulate in *Cfh*$^{+/-}$∼HFC mice (Figs. 3B, 3C), suggesting that C5a blockade is not sufficient to inhibit the accumulation of sub-RPE basal laminar deposits in the *Cfh*$^{+/-}$∼HFC mouse model.

We measured the damage to the RPE cells in aged *Cfh*$^{+/-}$ mice by quantifying dysmorphic, multinucleate RPE cells on RPE flat mounts stained with Hoechst 33342 to detect the nuclei and immunostained with the tight junction-associated protein, ZO-1, to reveal the cell borders (Fig. 3D). As previously reported, exposure to a HFC diet resulted in a statistically significant increase in the number of enlarged, multinucleate RPE cells in the *Cfh*$^{+/-}$ mice ($P < 0.05$) (Fig. 3E).[13] We found no statistical difference between *Cfh*$^{+/-}$∼HFC mice treated with and without anti-C5a therapy ($P > 0.05$) (Fig. 3E). These

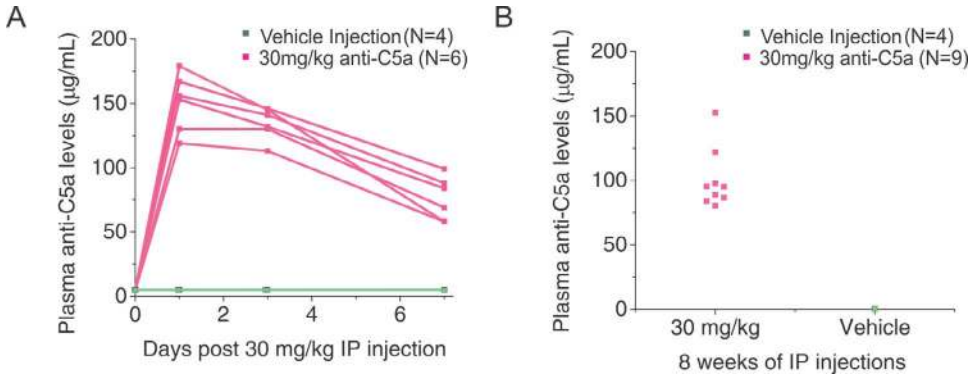

Figure 2. Sustained high levels of circulating antibodies are achieved with weekly injections of 30 mg/kg anti-C5a therapy. (**A**) Mice were injected IP with 30 mg/kg anti-C5a at day 0 and bled at days 1, 3, and 7 to establish the circulating antibody levels maintained throughout the week following weekly 30 mg/kg anti-C5a dosing. Antibody levels were determined by anti-C5a ELISA on plasma samples. (**B**) At the end of 8 weeks, most mice treated with 30 mg/kg anti-C5a maintained high circulating levels of anti-C5a therapy.

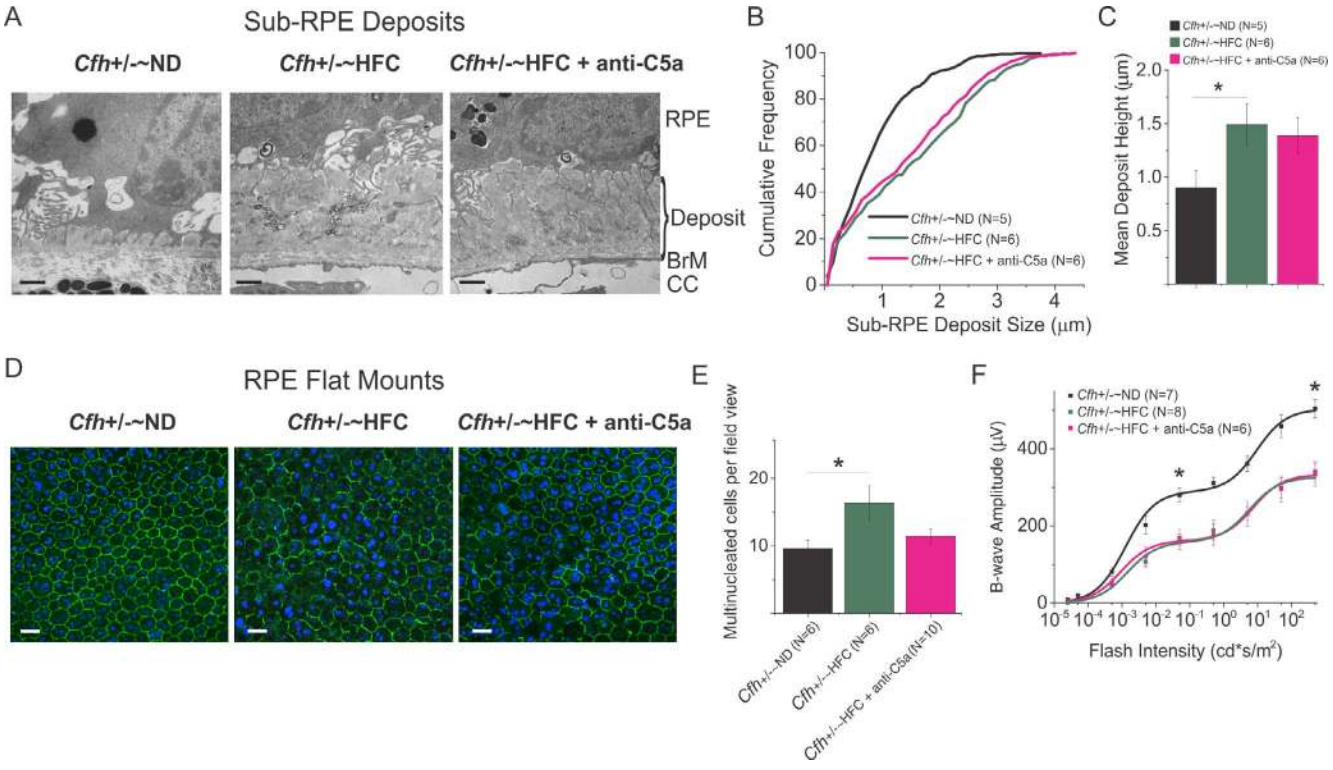

Figure 3. Anti-C5a therapy does not affect dry AMD-like features in $Cfh^{+/-}$~HFC mice. (**A**) Representative transmission electron micrograph images of basal laminar deposits along Bruch's membrane (BrM). Large (>2 µm) deposits were often seen in the $Cfh^{+/-}$~HFC and $Cfh^{+/-}$~HFC mice treated with 30 mg/kg anti-C5a, while only minimal sub-RPE deposit could be detected in aged-matched $Cfh^{+/-}$ fed a normal diet ($Cfh^{+/-}$~ND). *Scale bars*: 1 µm. (**B**) Quantitative analysis of sub-RPE basal laminar deposits using cumulative frequency curves shows that no change in the size of sub-RPE basal laminar deposits was detected between $Cfh^{+/-}$~HFC mice and $Cfh^{+/-}$~HFC mice treated with anti-C5a therapy. (**C**) Quantitative analysis of mean deposit size per mouse shows no difference could be detected between $Cfh^{+/-}$~HFC mice and $Cfh^{+/-}$~HFC mice treated with anti-C5a therapy. *Asterisk* (*) indicates statistical significance at $P = 0.05$ by Student's *t*-test analysis. (**D**) Confocal fluorescence images of central RPE flat mounts from >90-week-old $Cfh^{+/-}$ mice fed a ND or HFC diet treated with 0 or 30 mg/kg anti-C5a that were stained with Hoechst 33342 (*blue*, nuclei) and anti-ZO-1 (*green*) and imaged with the RPE apical side up with the neural retina removed. In $Cfh^{+/-}$~HFC mice there are many more enlarged, multinucleate cells following HFC diet, whereas in some mice RPE cells appear to be protected from damage in $Cfh^{+/-}$~HFC mice treated with 30 mg/kg anti-C5a. *Scale bars*: 20 µm. (**E**) Quantification of multinucleate (nuclei $\geq$ 3) RPE cells per field view demonstrates that some $Cfh^{+/-}$~HFC mice treated with 30 mg/kg anti-C5a appear to be protected, but no statistically significant differences are detected. *Asterisk* (*) indicates statistical significance at $P < 0.05$ by Student's *t*-test analysis. (**F**) Scotopic electroretinogram (ERG) flash responses in $Cfh^{+/-}$ fed a ND or HFC diet treated with 0 or 30 mg anti-C5a therapy. Stimulus-response curves of b-wave amplitudes. Data are expressed as mean ± SE of the stimulus-response curve overlaid with B = (Bmax1* I / I + I1) + (Bmax2 * I / I + I2) comparing ND (*black*), HFC (*green*), and HFC treated with 30 mg/kg anti-C5a (*pink*). $Cfh^{+/-}$~HFC mice ± anti-C5a treatment were significantly worse following HFC diet. *Asterisk* (*) indicates statistical significance at $P <$ 0.05 by Student's *t*-test analysis for the indicated flash intensities comparing $Cfh^{+/-}$~ND and $Cfh^{+/-}$~HFC.

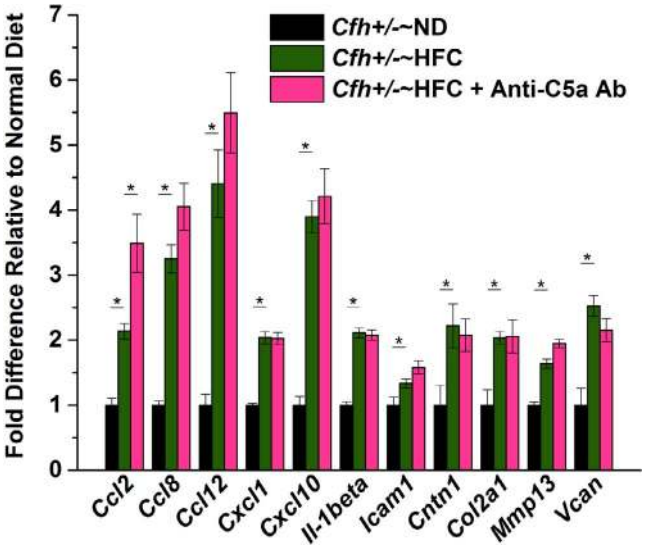

FIGURE 4. HFC-induced expression of inflammatory and ECM-related genes in eyecups of aged $Cfh^{+/-}$ mice is not decreased by anti-C5a therapy. Expression of inflammatory and ECM-related genes in the RPE/choroid/sclera of $Cfh^{+/-}$~ND, $Cfh^{+/-}$~HFC, and $Cfh^{+/-}$~HFC + anti-C5a therapy mice. Increases in the mRNA expression of *Ccl2*, *Ccl8*, *Ccl12*, *Cxcl1*, *Cxcl10*, *Il-1beta*, *Icam1*, *Cntn1*, *Col2a1*, *Mmp13*, and *Vcan* were detected in both $Cfh^{+/-}$~HFC and $Cfh^{+/-}$~HFC mice treated with anti-C5a antibody and suggest that the HFC-associated increases of these genes is C5a independent. Interestingly, statistically significant increases in *Ccl2* were observed in $Cfh^{+/-}$~HFC mice treated with anti-C5a antibody compared to $Cfh^{+/-}$~HFC mice. Data are presented as normalized averages of triplicate RT-PCR reactions relative to four pooled eyecups from normal diet age-matched $Cfh^{+/-}$ mice. *Error bars* represent standard deviations. *Asterisk* (*) represents statistical significance at $P < 0.05$ using ANOVA statistical analysis with post hoc Tukey test comparing gene expression between four pooled eyecups of normal and HFC diet-fed mice or mice fed a HFC diet and those fed a HFC diet and treated with anti-C5a.

data demonstrate that anti-C5a therapy does not appear to protect mice from the RPE dysmorphogenesis seen in the $Cfh^{+/-}$~HFC mice.

As previously reported, $Cfh^{+/-}$ mice develop a statistically significant decline in scotopic visual function measured by electroretinography following 8 weeks of HFC diet compared to age-matched wild-type controls on HFC.[13] Systemic anti-C5a immunotherapy did not protect the $Cfh^{+/-}$~HFC mice from losing visual function (Fig. 3F).

HFC Diet Increases Expression of Inflammation and ECM Genes in the Eyecups of Aged $Cfh^{+/-}$ Mice

Based on the association between AMD-like pathology in the $Cfh^{+/-}$~HFC model with RPE/choroid inflammation and accumulation of ECM debris,[13] we analyzed expression of inflammatory and ECM genes using pathway-focused PCR arrays. Transcript levels for inflammatory and ECM remodeling genes were measured using PCR arrays of inflammatory and ECM genes to characterize changes in these pathways that occur in the posterior eyecup (RPE/choroid/sclera) of $Cfh^{+/-}$~HFC mice compared to $Cfh^{+/-}$ mice fed a normal diet ($Cfh^{+/-}$~ND). These arrays contain 84 genes and have previously been used to interrogate the expression of inflammatory and ECM genes in the murine eye.[44,45] A complete list of inflammatory and ECM genes and their fold changes is included in Supplementary Tables S1 and S2, respectively. Sixty-five inflammatory genes were detected in the pooled $Cfh^{+/-}$ RPE/choroid eyecup RNA samples; of these, 35 genes were unchanged, 29 genes were upregulated, and only 1 gene (*Ccl11*) was downregulated due to the HFC diet (Supplementary Table S1 and Fig. S2A). Similarly, 80 ECM genes were detected, of which 29 were unchanged, 47 were upregulated, and 4 were downregulated in response to the HFC diet (Supplementary Table S2 and Fig. S2B). These results indicate that there is increased expression of inflammatory and ECM genes in the aged $Cfh^{+/-}$ due to the HFC diet.

Anti-C5a Therapy Does Not Ameliorate HFC-Induced Inflammatory and ECM Gene Expression in the Eyecups of Aged $Cfh^{+/-}$ Mice

After obtaining a profile of inflammatory and ECM gene expression in the eyecups isolated from aged $Cfh^{+/-}$ mice fed the HFC diet, we validated the expression of a subset of these genes that had a fold change of 1.25 or more (Fig. 4). We also investigated the effect of blocking C5a on the expression of these same genes in $Cfh^{+/-}$~HFC mice (Fig. 4). There was a statistically significant increase in the expression of the inflammatory genes *Ccl2*, *Ccl8*, *Ccl12*, *Cxcl1*, *Cxcl10*, *Il-1beta*, and the ECM genes *Cntn1*, *Col2a1*, *Mmp13*, *Vcan* plus *Icam1* (gene for an intracellular adhesion molecule on ECM array) in the pooled eyecups of $Cfh^{+/-}$~HFC mice compared to $Cfh^{+/-}$~ND mice (Fig. 4). Expression of these sampled genes was increased in eyecups of the $Cfh^{+/-}$~HFC mice treated with anti-C5a, but no decreases were observed comparing $Cfh^{+/-}$~HFC mice and $Cfh^{+/-}$~HFC mice treated with anti-C5a (Fig. 4). Interestingly, of these there was only a statistically significant increase in *Ccl2* in $Cfh^{+/-}$~HFC mice treated with anti-C5a antibody compared to $Cfh^{+/-}$~HFC mice (Fig. 4). These findings show that C5a does not appear to contribute to the increased expression of ECM or inflammatory genes in the eyecups of $Cfh^{+/-}$~HFC mice.

Complement Component 5a (C5a) Receptor Is Predominantly Expressed in Mouse and Human Choroid but Not in Mouse and Human RPE

C5a has been shown to increase the expression of inflammatory and ECM remodeling genes such as *Ccl2* and *Icam1* in the murine posterior eye[19,46] but the anti-C5a therapy did not change the expression of these genes in the eyecups of $Cfh^{+/-}$~HFC mice. To localize the effect of the anti-C5a therapy in the posterior eye we investigated the relative expression levels of the C5a receptor, complement component 5a receptor 1 (*C5aR1*), in mouse and human retina, RPE, and choroid/sclera and human choroid tissues. The relative expression of *C5aR1* was measured by RT-PCR in different regions of the mouse eye using posterior eye tissue-enriched RNA isolated from the neural retina, RPE, and choroid. We examined the expression of rhodopsin (*Rho*) (Fig. 5A), retinaldehyde-binding protein 1 (*Rlbp1*) (Fig. 5B), RPE-specific protein 65 kDa (*Rpe65*) (Fig. 5B), and tyrosine kinase with immunoglobulin and epidermal growth factor homology domain-2 (*Tie2*) (Fig. 5C) to confirm the enrichment of the retinal, RPE, and choroidal/scleral RNA samples, respectively. The majority of *C5ar1* (Fig. 5D) was in choroid/sclera-enriched samples compared to RPE-enriched and neural retina samples.

Based on the low levels of *C5ar1* transcript detected in the mouse RPE-enriched sample compared to the amount detected in the choroid/sclera, it is possible that the RPE signal is due to contamination of the mouse RPE-enriched RNA with choroidal RNA, and that murine RPE cells do not express the *C5ar1*. To support this, we examined the relative expression of the human *C5AR1* in human RPE- and choroid-enriched RNA samples as well as ARPE-19 cells, an immortalized human RPE

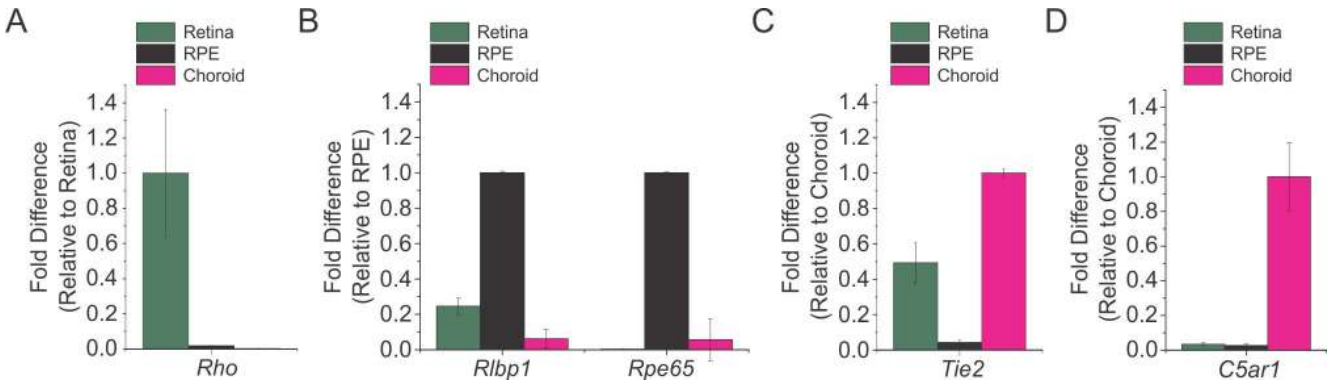

Figure 5. *C5ar1* expression in mouse retina, RPE, and choroid/sclera. RNA was isolated from mouse retinal, RPE, and choroid/scleral tissue. Enrichment of cell- or tissue-specific transcripts was tested by RT-PCR amplification of the genes coding for (**A**) rhodopsin (*Rho,* rod photoreceptor specific, retinal marker), (**B**) *Rlbp1* (*left*) and *Rpe65* (*right*, RPE markers), (**C**) *Tie2* (endothelial cell, choroid marker) and (**D**) *C5ar1*. Although *C5ar1* was detected in all the samples, the majority of *C5ar1* expression is confined to the choroid/sclera, suggesting that expression detected in the RPE is due to contamination from the choroid. The data represent two independent experiments.

cell line that has been shown to express *C5AR*.[22] The purity of the RPE- and choroid-enriched tissues we isolated was tested by RT-PCR, as described above, for human *RPE65* (Supplementary Fig. S3A), *RLBP1* (Supplementary Fig. S3A), and *TIE2* (Supplementary Fig. S3B). Expression of *RLBP1,* but not *RPE65*, was detected in ARPE-19 cells (Supplementary Fig. S3A) and confirms previously published findings.[47] Examination of *C5AR1* expression using these samples revealed no *C5AR1* expression in the human RPE-enriched sample while *C5AR1* was abundantly expressed in the human choroid-enriched sample (Supplementary Fig. S3C). Interestingly, there was no detection of *C5AR1* in ARPE-19 cells (Supplementary Fig. S3C). In summary, we conclude that the majority of *C5AR1* occurs in the choroid while there is little or no expression of *C5AR1* in the RPE.

Anti-C5a Therapy Ameliorates Classical Monocytosis Seen in *Cfh*$^{+/-}$∼HFC Mice

In our previous study of aged *Cfh*$^{+/-}$ and *Cfh*$^{-/-}$ mice fed a HFC diet we found a correlation between complement dysregulation in the *Cfh*$^{+/-}$ mice with peripheral monocytosis and increased MNPs in the choroid.[13] These findings made the *Cfh*$^{+/-}$∼HFC a relevant model to test the effects of anti-C5a therapy on monocyte levels and MNP recruitment to the choroid. In the peripheral blood an established gating strategy[13,38] was used to determine the percentage of classical and nonclassical monocytes (Fig. 6A).[13] As expected, polymorphonuclear leukocytes (PMNs) ($P < 0.05$), classical monocytes ($P < 0.05$), and nonclassical monocyte populations were increased in old *Cfh*$^{+/-}$ mice following 8 weeks of HFC diet compared to age-matched controls maintained on a ND. Interestingly, the classical monocyte population in the *Cfh*$^{+/-}$∼HFC mice was decreased following anti-C5a treatment, while PMNs were elevated and nonclassical monocytes were unchanged (Fig. 6B). Thus, systemic anti-C5a therapy ameliorates the classical monocytosis ($P < 0.05$) detected in the peripheral blood of *Cfh*$^{+/-}$ mice following HFC diet.

Anti-C5a Therapy Blocks Recruitment of Monocytes Into the Choroid

Intra- and extravascular flow cytometry was used to test the hypothesis that anti-C5a therapy blocks MNP recruitment in the RPE/choroid. We used a previously established gating strategy to distinguish the intra- and extravascular space using an intravascularly injected anti-CD45 antibody (Fig. 7A).[13] Within the extravascular space there were statistically significant increases in total leukocytes ($P < 0.05$), in PMNs, and within all MNP populations (Ly6C^{hi} [classical monocytes], Ly6C^{lo}, and CD64+, $P < 0.05$) in *Cfh*$^{+/-}$ mice following HFC diet (Fig. 7B). Anti-C5a therapy blocked the increases in total leukocytes ($P < 0.05$), PMNs, classical monocytes, and Ly6C^{lo} MNPs ($P < 0.05$) but not CD64+ MNPs within the RPE/choroid extravascular space (Fig. 7B). Together these results demonstrate that systemic anti-C5a therapy blocks monocyte recruitment to the choroid of *Cfh*$^{+/-}$∼HFC mice.

Discussion

AMD is a multifactorial disease characterized by early features including reduced rod-mediated light sensitivity, slower dark adaptation, RPE pigmentary changes, and drusen accumulation.[2–4,48] Genetic, biochemical, and clinical studies have converged to implicate the complement system in the pathogenesis of AMD development and progression. However, understanding the role of complement in the pathogenesis of AMD is critical for the development of novel therapies. We recently developed an early/intermediate dry AMD mouse model based on advanced age, alternative pathway dysregulation, and consumption of a HFC diet.[13] This aged *Cfh*$^{+/-}$∼HFC mouse model of early/intermediate dry AMD can be used to elucidate the roles of activated complement components and to test complement-based therapies in a model of AMD.

We have previously demonstrated that systemic immunotherapy targeting amyloid beta, a known component of drusen[49–51] that induces complement activation,[49,50,52,53] can protect from development of an AMD phenotype in the *APOE4* mouse model of AMD.[54] Using a similar approach, in this study we tested the pharmacologic effects of a monoclonal anti-C5a therapy in aged male *Cfh*$^{+/-}$∼HFC mice. Aged *Cfh*$^{+/-}$ fed a HFC diet have decreased scotopic ERG b-wave responses, increased RPE damage, increased sub-RPE basal laminar deposits, and increased expression of inflammatory and ECM genes. We show that anti-C5a therapy fails to ameliorate these HFC-induced pathologies in aged *Cfh*$^{+/-}$ mice. As a proof of drug efficacy, we used the $NaIO_3$ model of retinal degeneration and the laser-induced CNV model of wet AMD to confirm the therapeutic potential of systemically delivered anti-C5a antibody in the posterior eye. Although no complement therapies have been tested in the $NaIO_3$ model to date, our results from the laser-induced CNV model are supported by others.[8,23,24] Our data suggest that C5a blockade is not sufficient to stop the

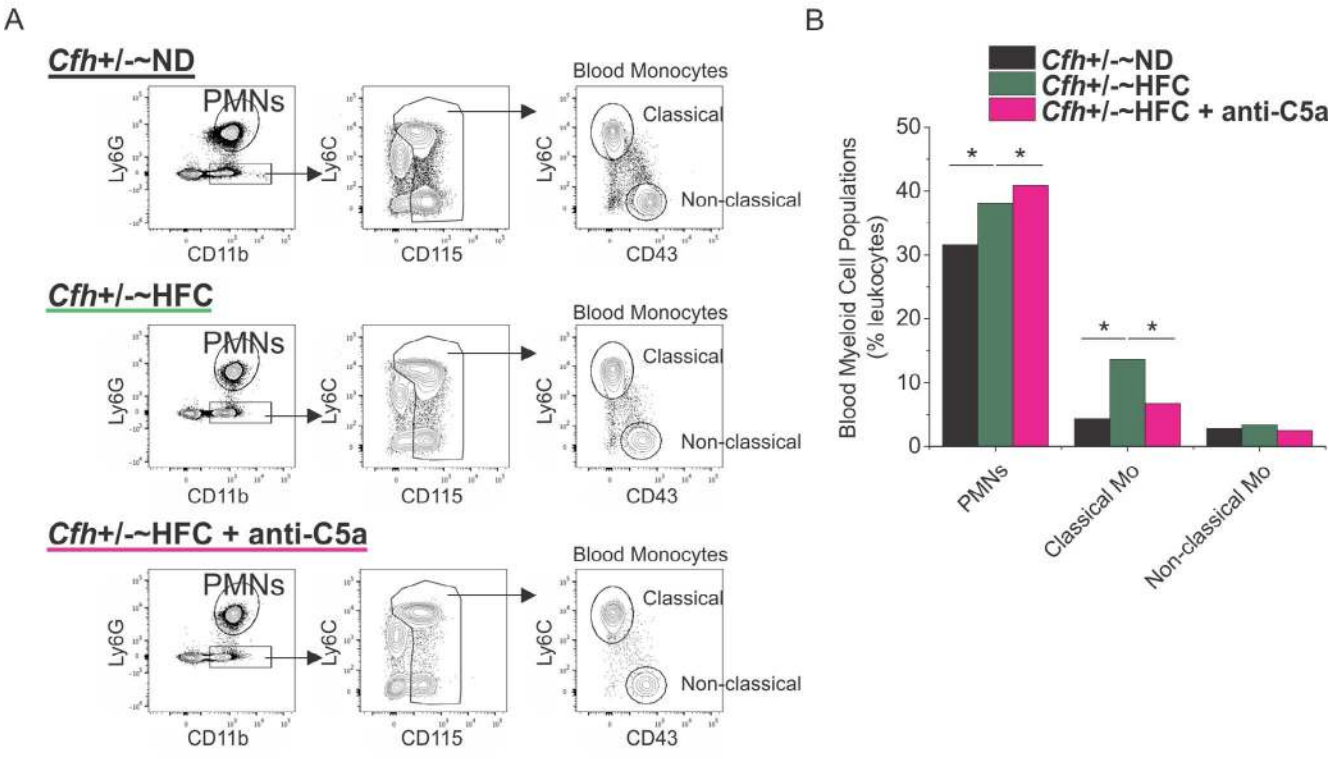

Figure 6. Increase in blood classical monocytes in $Cfh^{+/-}$~HFC mice is ameliorated by anti-C5a therapy. (**A**) Flow cytometry was performed on peripheral blood mononuclear phagocytes in $Cfh^{+/-}$~ND, $Cfh^{+/-}$~HFC, and $Cfh^{+/-}$~HFC + anti-C5a therapy. (**B**) An increase in the percentage of classical and nonclassical monocytes (Mo) was seen in $Cfh^{+/-}$ mice following HFC diet, and anti-C5a therapy ameliorated the classical monocytosis. *Asterisk* (*) represents statistical significance using χ^2 statistical analysis for $P < 0.05$. The data presented represent two independent experiments, each with a single pooled sample with three mice per group.

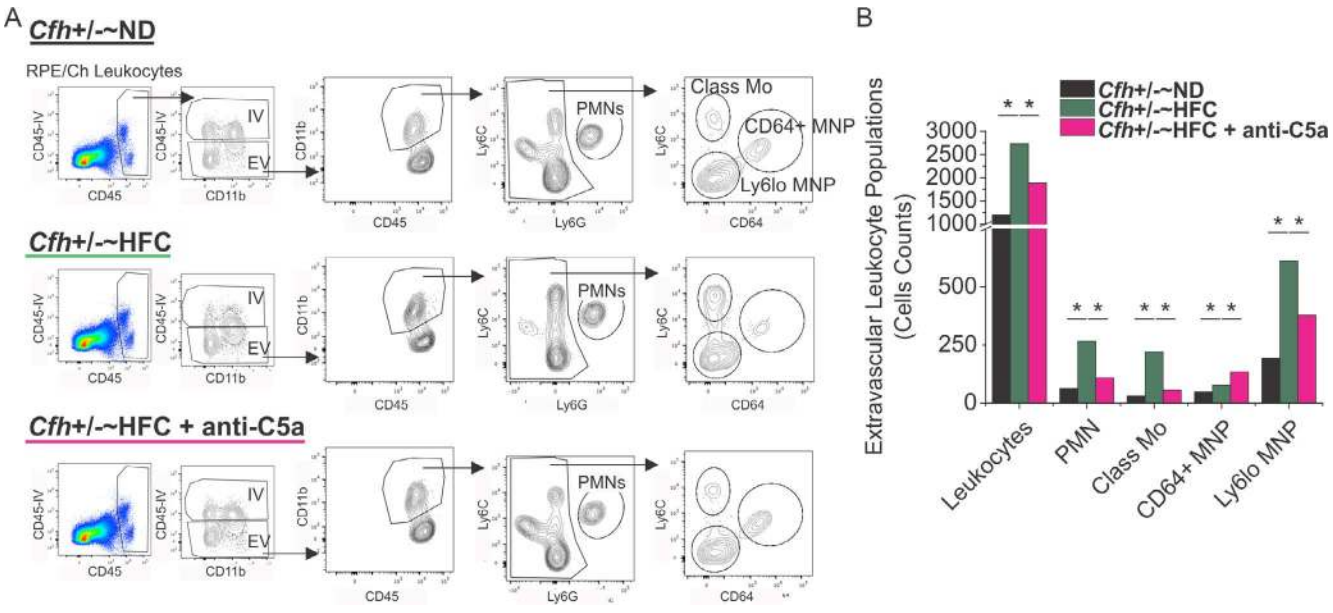

Figure 7. Extravascular choroidal mononuclear phagocytes are increased in $Cfh^{+/-}$~HFC mice and are ameliorated by anti-C5a therapy. (**A**) RPE/choroid leukocytes were gated for an intravascularly injected anti-CD45 antibody to distinguish the intra- and extravascular space. Gating for polymorphonuclear leukocytes (PMNs) and three previously established populations of mononuclear phagocyte (MNP) ($Ly6C^{hi}$ [Class Mo], $Ly6C^{lo}$, and CD64+) was performed.[64] (**B**) Within the extravascular space significant increases were seen in total leukocytes, PMNs, and all the MNP subpopulations (Class Mo, CD64+ MNP, and $Ly6C^{lo}$ MNP). Interestingly, anti-C5a therapy significantly blocked the extravasation of total leukocytes and PMNs, as well as Class Mo and $Ly6C^{lo}$ MNP subpopulations. *χ^2 test for $P < 0.05$. Data presented represent a single experiment using a pooled sample from three mice per group. A separate independent experiment was performed to confirm trends shown above. Class Mo, classical monocyte.

development of AMD-like pathologies in *Cfh*$^{+/-}$∼HFC mice and therefore may not be a viable treatment in early/intermediate dry AMD, although it shows promise as a potential mono- or combination therapy with anti-VEGF in wet AMD.

C5a is a potent anaphylatoxin critical in the recruitment and activation of immune cells to sites of tissue damage. In wet AMD a prominent pathologic hallmark is CNV where choroidal blood vessels proliferate and migrate through BrM into the sub-RPE and subretinal space causing leakage, fibrosis, and eventual tissue damage.[12] A role of immune cells such as dendritic cells,[55] γδ T-cells,[23,56] neutrophils,[57] and macrophages[58,59] in CNV has been implicated using the laser-induced CNV mouse model of wet AMD. All of these immune cells have been shown to express the C5a receptor, C5aR1.[60] Therefore, targeting C5a with either antibodies or aptamers should diminish the exudative lesion size by targeting immune cell populations in the laser-induced CNV mouse model of wet AMD as confirmed by our results and others.[8,23,24]

Recruitment of immune cells in early/intermediate dry AMD mouse models has been reported, but the role of immune cells on the development of pathologies in these mouse models is not well understood.[61] This study is the first to examine a role for immune cells specifically recruited by C5a during the development of early/intermediate dry AMD-like pathologies in vivo. Our results suggest that recruitment of total leukocytes, PMNs, classical monocytes, and Ly6C^{lo} MNPs is sensitive to C5a blockade, but these changes are not sufficient to block the early/intermediate dry AMD-like pathologies seen in *Cfh*$^{+/-}$∼HFC mice.

In the current study, there was no significant protective effect from RPE damage or vision loss in *Cfh*$^{+/-}$∼HFC mice treated with systemic immunotherapy blocking C5a. There was increased expression of a subset of inflammation- and ECM-related genes in the RPE/choroid/sclera isolated from *Cfh*$^{+/-}$∼HFC compared to *Cfh*$^{+/-}$∼ND, but this increase was not affected by anti-C5a treatment. Because anti-C5a therapy successfully blocked immune cell recruitment to the choroid we suspect that the increased inflammatory and ECM gene expression detected originates from the choroid and/or RPE, and therefore, we measured the relative expression of the *C5AR1* in posterior eye tissues. Previous studies have examined the expression of the *C5AR1* in human donor eye tissue and found *C5AR1* expression in the choroid and retina[19] as well as in the immortalized human RPE cell line, ARPE-19.[22] We therefore measured the relative *C5ar1* levels in RPE, choroid, and retina isolated from mouse eyes. We found much higher *C5ar1* expression in isolated choroid RNA compared to the RPE and retina RNA obtained from C57BL/6J mice. Although low levels of *C5ar1* expression were detected in the isolated RPE RNA, it is likely that this *C5ar1* expression is due to contamination from the choroid based on the signal detected for the endothelial cell marker, *Tie2*, in the RPE-enriched sample. We obtained similar results using RPE and choroid RNA isolated from a human donor eye and failed to detect *C5AR1* expression in ARPE-19 cells. The *C5AR1* expression in ARPE-19 measured by RT-PCR by Cortright et al.[22] may well be due to genomic DNA contamination since the primers used were nested within a single exon (exon 2). Thus, under normal conditions the majority of *C5ar1* expression is confined to the choroid while RPE cells do not appear to express *C5ar1* in vivo. As a consequence, blocking C5a would not affect the HFC-mediated damage occurring to the RPE and may help explain why anti-C5a therapy did not ameliorate the AMD-like pathologies seen in *Cfh*$^{+/-}$∼HFC mice.

Our results suggest that other components of the complement cascade such as the anaphylatoxin C3a and/or the terminal membrane attack complex (MAC) may be more important for the development of early AMD-like pathologies in *Cfh*$^{+/-}$∼HFC mice. A model of Malattia Leventinese/Doyne honeycomb retinal dystrophy, an inherited macular degeneration, using *EFEMP1*^{R345W} knock-in mice[62] and RPE cell culture,[63] suggests that sub-RPE deposit formation is dependent on complement component 3a (C3a), but not on C5a. These results are consistent with our findings that anti-C5a therapy did not affect sub-RPE deposit formation. In addition, we have previously shown that CFH levels regulate lipoprotein binding and remove endogenous human lipoproteins in BrM.[13] In the absence of CFH or decreased CFH, lipoproteins can accumulate and provide a scaffold in which complement activation can occur in the sub-RPE region of the posterior eye and lead to the development of early/intermediate dry AMD. Furthermore, there could be a role of the MAC in our animal model that would not be blocked by anti-C5a therapy.

In summary, while no mouse model can faithfully recapitulate all the insults and responses likely to play a role in the development of early/intermediate dry AMD, this model does combine the effects of aging, complement dysregulation, and changes in lipid homeostasis—three known factors involved in AMD pathogenesis. With this caveat, targeting the complement activation product C5a is not sufficient to ameliorate the pathologies seen in the aged *Cfh*$^{+/-}$∼HFC mouse model of early/intermediate dry AMD; however, it is able to block the recruitment of MNPs to the RPE-choroid and decrease lesion size in the laser-induced CNV mouse model of wet AMD. Future studies will investigate the role of C3a and MAC in the development of the AMD-like phenotype observed in *Cfh*$^{+/-}$∼HFC and determine if pharmacologically targeting C3a or MAC or both could be a viable therapy for early/intermediate dry AMD.

Acknowledgments

The authors thank Ying Hao and Marybeth Groelle for their expert technical assistance and Rose Matthews and Joan Kalnitsky for their assistance with flow cytometry. We acknowledge Wei Li, Gabriel Berstein, Huilan Gao, and Laird Bloom of Pfizer, Inc., for providing the neutralizing anti-C5a antibody 4C9 and Li Mei for helping engineer the higher-affinity variant of 4C9 used in this study. We also thank Karen Christopherson of Pfizer, Inc., for her insights and helpful suggestions during the initiation and development of this project.

Supported by National Eye Institute Grants R01 EY026161 (CBR) and P30 EY005722, T32 GM007171-Medical Scientist Training Program (CBT), an unrestricted grant from Research to Prevent Blindness (to the Duke Eye Center), a grant from the BrightFocus Foundation (MK), and a grant from the Foundation Fighting Blindness (CBR). Pfizer, Inc., owns the intellectual properties of the antibodies described in this study.

Disclosure: **C.B. Toomey**, None; **M. Landowski**, None; **M. Klingeborn**, None; **U. Kelly**, None; **J. Deans**, None; **H. Dong**, Pfizer, Inc. (E); **O. Harrabi**, Pfizer, Inc. (E); **T. Van Blarcom**, Pfizer, Inc. (E); **Y.A. Yeung**, Pfizer, Inc. (E); **R. Grishanin**, Pfizer, Inc. (E); **J.C. Lin**, Pfizer, Inc. (E); **D.R. Saban**, None; **C. Bowes Rickman**, Pfizer, Inc. (F)

References

1. Chew EY, Clemons TE, Agron E, et al. Ten-year follow-up of age-related macular degeneration in the age-related eye disease study: AREDS report no. 36. *JAMA Ophthalmol*. 2014;132:272–277.
2. Rudnicka AR, Jarrar Z, Wormald R, Cook DG, Fletcher A, Owen CG. Age and gender variations in age-related macular degeneration prevalence in populations of European ancestry: a meta-analysis. *Ophthalmology*. 2012;119:571–580.

3. van Leeuwen R, Boekhoorn S, Vingerling JR, et al. Dietary intake of antioxidants and risk of age-related macular degeneration. *JAMA*. 2005;294:3101–3107.
4. VandenLangenberg GM, Mares-Perlman JA, Klein R, Klein BE, Brady WE, Palta M. Associations between antioxidant and zinc intake and the 5-year incidence of early age-related maculopathy in the Beaver Dam Eye Study. *Am J Epidemiol*. 1998;148:204–214.
5. Tan PL, Bowes Rickman C, Katsanis N. AMD and the alternative complement pathway: genetics and functional implications. *Hum Genomics*. 2016;10:23.
6. Johnson LV, Ozaki S, Staples MK, Erickson PA, Anderson DH. A potential role for immune complex pathogenesis in drusen formation. *Exp Eye Res*. 2000;70:441–449.
7. Johnson LV, Leitner WP, Staples MK, Anderson DH. Complement activation and inflammatory processes in Drusen formation and age related macular degeneration. *Exp Eye Res*. 2001;73:887–896.
8. Nozaki M, Raisler BJ, Sakurai E, et al. Drusen complement components C3a and C5a promote choroidal neovascularization. *Proc Natl Acad Sci U S A*. 2006;103:2328–2333.
9. Crabb JW, Miyagi M, Gu X, et al. Drusen proteome analysis: an approach to the etiology of age-related macular degeneration. *Proc Natl Acad Sci U S A*. 2002;99:14682–14687.
10. Fritsche LG, Fariss RN, Stambolian D, Abecasis GR, Curcio CA, Swaroop A. Age-related macular degeneration: genetics and biology coming together. *Annu Rev Genomics Hum Genet*. 2014;15:151–171.
11. Yaspan BL, Williams DF, Holz FG, et al. Targeting factor D of the alternative complement pathway reduces geographic atrophy progression secondary to age-related macular degeneration. *Sci Transl Med*. 2017;9:eaaf1443.
12. Miller JW. Age-related macular degeneration revisited – piecing the puzzle: the LXIX Edward Jackson memorial lecture. *Am J Ophthalmol*. 2013;155:1–35.e13.
13. Toomey CB, Kelly U, Saban DR, Bowes Rickman C. Regulation of age-related macular degeneration-like pathology by complement factor H. *Proc Natl Acad Sci U S A*. 2015;112:E3040–E3049.
14. Pickering MC, Cook HT, Warren J, et al. Uncontrolled C3 activation causes membranoproliferative glomerulonephritis in mice deficient in complement factor H. *Nat Genet*. 2002;31:424–428.
15. Merle NS, Noe R, Halbwachs-Mecarelli L, Fremeaux-Bacchi V, Roumenina LT. Complement system part II: role in immunity. *Front Immunol*. 2015;6:257.
16. Scholl HP, Charbel Issa P, Walier M, et al. Systemic complement activation in age-related macular degeneration. *PLoS One*. 2008;3:e2593.
17. Reynolds R, Hartnett ME, Atkinson JP, Giclas PC, Rosner B, Seddon JM. Plasma complement components and activation fragments: associations with age-related macular degeneration genotypes and phenotypes. *Invest Ophthalmol Vis Sci*. 2009;50:5818–5827.
18. Lechner J, Chen M, Hogg RE, et al. Higher plasma levels of complement C3a, C4a and C5a increase the risk of subretinal fibrosis in neovascular age-related macular degeneration: complement activation in AMD. *Immun Ageing*. 2016;13:4.
19. Skeie JM, Fingert JH, Russell SR, Stone EM, Mullins RF. Complement component C5a activates ICAM-1 expression on human choroidal endothelial cells. *Invest Ophthalmol Vis Sci*. 2010;51:5336–5342.
20. Liu B, Wei L, Meyerle C, et al. Complement component C5a promotes expression of IL-22 and IL-17 from human T cells and its implication in age-related macular degeneration. *J Transl Med*. 2011;9:1–12.
21. Cao S, Wang JC, Gao J, et al. CFH Y402H polymorphism and the complement activation product C5a: effects on NF-kappaB activation and inflammasome gene regulation. *Br J Ophthalmol*. 2016;100:713–718.
22. Cortright DN, Meade R, Waters SM, Chenard BL, Krause JE. C5a, but not C3a, increases VEGF secretion in ARPE-19 human retinal pigment epithelial cells. *Curr Eye Res*. 2009;34:57–61.
23. Coughlin B, Schnabolk G, Joseph K, et al. Connecting the innate and adaptive immune responses in mouse choroidal neovascularization via the anaphylatoxin C5a and gammadeltaT-cells. *Sci Rep*. 2016;6:23794.
24. Brockmann C, Brockmann T, Dege S, et al. Intravitreal inhibition of complement C5a reduces choroidal neovascularization in mice. *Graefes Arch Clin Exp Ophthalmol*. 2015;253:1695–1704.
25. Mattapallil MJ, Wawrousek EF, Chan CC, et al. The Rd8 mutation of the Crb1 gene is present in vendor lines of C57BL/6N mice and embryonic stem cells, and confounds ocular induced mutant phenotypes. *Invest Ophthalmol Vis Sci*. 2012;53:2921–2927.
26. Van Blarcom T, Rossi A, Foletti D, et al. Precise and efficient antibody epitope determination through library design, yeast display and next-generation sequencing. *J Mol Biol*. 2015;427:1513–1534.
27. Rajpal A, Beyaz N, Haber L, et al. A general method for greatly improving the affinity of antibodies by using combinatorial libraries. *Proc Natl Acad Sci U S A*. 2005;102:8466–8471.
28. Boder ET, Wittrup KD. Yeast surface display for screening combinatorial polypeptide libraries. *Nat Biotechnol*. 1997;15:553–557.
29. Uehara H, Cho Y, Simonis J, et al. Dual suppression of hemangiogenesis and lymphangiogenesis by splice-shifting morpholinos targeting vascular endothelial growth factor receptor 2 (KDR). *FASEB J*. 2012;27:76–85.
30. Enzmann V, Row BW, Yamauchi Y, et al. Behavioral and anatomical abnormalities in a sodium iodate-induced model of retinal pigment epithelium degeneration. *Exp Eye Res*. 2006;82:441–448.
31. Lambert V, Lecomte J, Hansen S, et al. Laser-induced choroidal neovascularization model to study age-related macular degeneration in mice. *Nat Protoc*. 2013;8:2197–2211.
32. Ding JD, Kelly U, Landowski M, et al. Expression of human complement factor H prevents age-related macular degeneration-like retina damage and kidney abnormalities in aged cfh knockout mice. *Am J Pathol*. 2015;185:29–42.
33. Livak KJ, Schmittgen TD. Analysis of relative gene expression data using real-time quantitative PCR and the 2(-Delta C(T)) Method. *Methods*. 2001;25:402–408.
34. Kurihara T, Westenskow PD, Gantner ML, et al. Hypoxia-induced metabolic stress in retinal pigment epithelial cells is sufficient to induce photoreceptor degeneration. *Elife*. 2016;5:e14319.
35. Xin-Zhao Wang C, Zhang K, Aredo B, Lu H, Ufret-Vincenty RL. Novel method for the rapid isolation of RPE cells specifically for RNA extraction and analysis. *Exp Eye Res*. 2012;102:1–9.
36. Choudhary M, Ding JD, Qi X, et al. PPARbeta/delta selectively regulates phenotypic features of age-related macular degeneration. *Aging*. 2016;8:1952–1978.
37. O'Koren EG, Mathew R, Saban DR. Fate mapping reveals that microglia and recruited monocyte-derived macrophages are definitively distinguishable by phenotype in the retina. *Sci Rep*. 2016;6:20636.
38. Carlin LM, Stamatiades EG, Auffray C, et al. Nr4a1-dependent Ly6C(low) monocytes monitor endothelial cells and orchestrate their disposal. *Cell*. 2013;153:362–375.
39. Franco LM, Zulliger R, Wolf-Schnurrbusch UE, et al. Decreased visual function after patchy loss of retinal pigment epithelium induced by low-dose sodium iodate. *Invest Ophthalmol Vis Sci*. 2009;50:4004–4010.

Investigative Ophthalmology & Visual Science

40. Wang J, Iacovelli J, Spencer C, Saint-Geniez M. Direct effect of sodium iodate on neurosensory retina. *Invest Ophthalmol Vis Sci*. 2014;55:1941–1953.
41. Ishibashi T, Miller H, Orr G, Sorgente N, Ryan SJ. Morphologic observations on experimental subretinal neovascularization in the monkey. *Invest Ophthalmol Vis Sci*. 1987;28:1116–1130.
42. Poor SH, Qiu Y, Fassbender ES, et al. Reliability of the mouse model of choroidal neovascularization induced by laser photocoagulation. *Invest Ophthalmol Vis Sci*. 2014;55:6525–6534.
43. Hageman GS, Luthert PJ, Victor Chong NH, Johnson LV, Anderson DH, Mullins RF. An integrated hypothesis that considers drusen as biomarkers of immune-mediated processes at the RPE-Bruch's membrane interface in aging and age-related macular degeneration. *Prog Retin Eye Res*. 2001;20:705–732.
44. Kuny S, Gaillard F, Sauve Y. Differential gene expression in eyecup and retina of a mouse model of Stargardt-like macular dystrophy (STGD3). *Invest Ophthalmol Vis Sci*. 2012;53:664–675.
45. Tsau C, Ito M, Gromova A, Hoffman MP, Meech R, Makarenkova HP. Barx2 and Fgf10 regulate ocular glands branching morphogenesis by controlling extracellular matrix remodeling. *Development*. 2011;138:3307–3317.
46. Ambati J, Anand A, Fernandez S, et al. An animal model of age-related macular degeneration in senescent Ccl-2- or Ccr-2-deficient mice. *Nat Med*. 2003;9:1390–1397.
47. Carr AJ, Vugler AA, Yu L, et al. The expression of retinal cell markers in human retinal pigment epithelial cells and their augmentation by the synthetic retinoid fenretinide. *Mol Vis*. 2011;17:1701–1715.
48. Chew EY, Clemons TE, Agron E, et al. Ten-year follow-up of age-related macular degeneration in the Age-Related Eye Disease Study: AREDS Report No. 36. *JAMA Ophthalmol*. 2014;132:272–277.
49. Anderson DH, Talaga KC, Rivest AJ, Barron E, Hageman GS, Johnson LV. Characterization of beta amyloid assemblies in drusen: the deposits associated with aging and age-related macular degeneration. *Exp Eye Res*. 2004;78:243–256.
50. Dentchev T, Milam AH, Lee VM, Trojanowski JQ, Dunaief JL. Amyloid-beta is found in drusen from some age-related macular degeneration retinas, but not in drusen from normal retinas. *Mol Vis*. 2003;9:184–190.
51. Johnson LV, Leitner WP, Rivest AJ, Staples MK, Radeke MJ, Anderson DH. The Alzheimer's A beta-peptide is deposited at sites of complement activation in pathologic deposits associated with aging and age-related macular degeneration. *Proc Natl Acad Sci U S A*. 2002;99:11830–11835.
52. Kurji KH, Cui JZ, Lin T, et al. Microarray analysis identifies changes in inflammatory gene expression in response to amyloid-beta stimulation of cultured human retinal pigment epithelial cells. *Invest Ophthalmol Vis Sci*. 2010;51:1151–1163.
53. Wang J, Ohno-Matsui K, Yoshida T, et al. Amyloid-beta up-regulates complement factor B in retinal pigment epithelial cells through cytokines released from recruited macrophages/microglia: another mechanism of complement activation in age-related macular degeneration. *J Cell Physiol*. 2009;220:119–128.
54. Ding JD, Johnson LV, Herrmann R, et al. Anti-amyloid therapy protects against retinal pigmented epithelium damage and vision loss in a model of age-related macular degeneration. *Proc Natl Acad Sci U S A*. 2011;108:E279–E287.
55. Nakai K, Fainaru O, Bazinet L, et al. Dendritic cells augment choroidal neovascularization. *Invest Ophthalmol Vis Sci*. 2008;49:3666–3670.
56. Hasegawa E, Sonoda KH, Shichita T, et al. IL-23-independent induction of IL-17 from gammadeltaT cells and innate lymphoid cells promotes experimental intraocular neovascularization. *J Immunol*. 2013;190:1778–1787.
57. Zhou J, Pham L, Zhang N, et al. Neutrophils promote experimental choroidal neovascularization. *Mol Vis*. 2005;11:414–424.
58. Espinosa-Heidmann DG, Suner IJ, Hernandez EP, Monroy D, Csaky KG, Cousins SW. Macrophage depletion diminishes lesion size and severity in experimental choroidal neovascularization. *Invest Ophthalmol Vis Sci*. 2003;44:3586–3592.
59. Caicedo A, Espinosa-Heidmann DG, Pina Y, Hernandez EP, Cousins SW. Blood-derived macrophages infiltrate the retina and activate Müller glial cells under experimental choroidal neovascularization. *Exp Eye Res*. 2005;81:38–47.
60. Monk PN, Scola AM, Madala P, Fairlie DP. Function, structure and therapeutic potential of complement C5a receptors. *Br J Pharmacol*. 2007;152:429–448.
61. Pennesi ME, Neuringer M, Courtney RJ. Animal models of age related macular degeneration. *Mol Aspects Med*. 2012;33:487–509.
62. Garland DL, Fernandez-Godino R, Kaur I, et al. Mouse genetics and proteomic analyses demonstrate a critical role for complement in a model of DHRD/ML, an inherited macular degeneration. *Hum Mol Genet*. 2014;23:52–68.
63. Fernandez-Godino R, Garland DL, Pierce EA. A local complement response by RPE causes early-stage macular degeneration. *Hum Mol Genet*. 2015;24:5555–5569.
64. Souto FJ, Crispim JC, Ferreira SC, et al. Liver HLA-G expression is associated with multiple clinical and histopathological forms of chronic hepatitis B virus infection. *J Viral Hepat*. 2011;18:102–105.

Investigative Ophthalmology & Visual Science